

Document downloaded from:

<http://hdl.handle.net/10251/126496>

This paper must be cited as:

Bermúdez, V.; Ruiz-Rosales, S.; Novella Rosa, R.; Soto-Izquierdo, L. (2018). Effects of multiple injection strategies on gaseous emissions and particle size distribution in a two-stroke compression-ignition engine operating with the gasoline partially premixed combustion concept. *Proceedings of the Institution of Mechanical Engineers Part D Journal of Automobile Engineering*. 233(10):1-19. <https://doi.org/10.1177/0954407018802960>



The final publication is available at

<https://doi.org/10.1177/0954407018802960>

Copyright SAGE Publications

Additional Information

# Effects of multiple injection strategies on Particle emissions in a 2-stroke CI engine operating with gasoline Partially Premixed Combustion concept

Vicente Bermúdez, Santiago Ruiz, Ricardo Novella and Lian Soto

Universitat Politècnica de València, CMT-Motores Térmicos, Camino de Vera s/n, 46022 Valencia, Spain

## ABSTRACT

In order to improve performance and meet the requirements of the new pollutant emission regulations on Internal Combustion Engines (ICE), advanced combustion strategies have been investigated. The newly designed Partially Premixed Combustion (PPC) concept has demonstrated a potential in the reduction of NO<sub>x</sub> and particulate matter (PM) emissions, combined with high indicated efficiencies; while still retaining proper control over combustion process with different injection strategies.

In this study, parametric variations of injection pressure (IP), 2nd injection and 3rd injection timing were experimentally performed to analyze the effect of the injection strategy over air-to-fuel (AF) mixture process and its consequent impact on particle number (PN) emissions and particle size distribution. Tests were performed in a newly designed 2-stroke HSDI CI engine operating with the PPC concept using a commercial gasoline with Research Octane Number (RON) of 95. A Scanning Particle Sizer (SMPS) was used to measure the size distribution of engine-exhaust particle emissions. Three different steady-state operation modes in terms of indicated mean effective pressure (IMEP) and engine speed were investigated: 3.5 bar IMEP and 2000 rpm, 5.5 bar IMEP and 2000 rpm and 5.5 bar IMEP and 2500 rpm. The experiments showed an increase in PN emissions and a progressive shift in the particle size distribution towards larger sizes, increasing the accumulation-mode particles and reducing the nucleation-mode particles with the IP decrease and the 3rd injection timing delay. Additionally, the 2nd injection timing showed non-sensible variation of particle emissions.

## Keywords

2-Stroke engine; Gasoline PPC concept; PN emissions; Particle size distribution; Injection strategy

## 1. Introduction

Particulate matter (PM) is one of various pollutants emitted by internal combustion engines (ICE). This pollutant is defined as the heterogeneous mixture of solid and liquid particles with different characteristics or properties that vary in size, shape, surface, chemical composition, solubility, and origin (Hinds, 1999; Pope & Dockery, 2006). Numerous scientific studies have shown the health problems that provide the inhalation of PM emissions. In this regard, it has been shown that respiratory harmful effects caused by exposure to the exhaust gases are attributable more to its particulate content than to its gaseous content (Kim, Kabir, & Kabir, 2015; McCreanor et al., 2007). Some cardiovascular and carcinogenic problems are also associated with these particles, specifically with ultrafine particles that, due to their size and poor solubility, can pass from the lungs to the bloodstream (Davidson, Phalen, & Solomon, 2005; Oberdörster, Oberdörster, & Oberdörster, 2005).

## Nomenclature

AF	air-to-fuel	ICE	Internal Combustion Engines
aTDC	after top dead center	IMEP	Mean effective pressure
CA	Crank angle	IP	Injection pressure
CA10	Crank angle for 10% of fuel burnt	LDMA	Long Differential Mobility Analyzer
CA50	Crank angle for 50% of fuel burnt	NOx	Nitrogen oxides
CDC	Conventional Diesel Combustion	OLAP	Valve overlap
CI	Compression-ignition	PM	Particulate matter
CO <sub>2</sub>	Carbon dioxide	Pmax	Peak cylinder pressure
CPC	Condensation Particle Counter	PN	Particle number
DOCH	Double overhead camshafts	PPC	Partially Premixed Combustion
dM	Mass concentration	PSD	Particle Size Distributions
dN	Number concentration	RoHR	Rate of heat release
dP/dα	Pressure gradient	SIDI	Spark Ignited Direct Injection
ECU	Engine Control Unit	SoE	Start of energizing
EGR	Exhaust gas recirculation	SoC	Start of combustion
GMD	Geometric Mean Diameter	SMPS	Scanning Mobility Particle Sizer
HCCI	Homogeneous Charge Compression Ignition	ΔP	Pressure differential between intake and exhaust

Due to increasing social awareness about human health and the environment, the regulations in charge of the limits for the emissions produced by ICEs have evolved significantly. Regarding PM emissions, the latest EU legislations have defined as limit of  $6.0 \cdot 10^{11}$  #/km for particle number (PN) and 4.5 mg/km for PM mass. This reduction in pollutant limits have been applied in both spark ignited direct injection (SIDI) and compression-ignition (CI) engines.

To meet the requirements of the new pollutant emission regulations and while increasing the engine thermal efficiency, the vehicle manufacturers have invested heavily in the research and development of new combustion processes. Homogeneous Charge Compression Ignition (HCCI) combustion is one of these advanced combustion concepts that has been developed. In the HCCI combustion, the fuel is injected very early during the intake stroke or in the intake manifold, giving it sufficient time to mix completely with air, providing a homogenous charge that is compressed until the auto-ignites. Under these conditions the combustion process occurs by spontaneous auto-ignition at multiple points throughout the charge volume, without a diffusion flame [typical in Conventional Diesel Combustion (CDC)] and with the introduction exhaust gas recirculation (EGR), the nitrogen oxides (NOx) and PM emissions decrease considerably (Jia, Li, Xie, & Wang, 2013; A. P. Singh & Agarwal, 2012; G. Singh, Singh, & Agarwal, 2014). However, the auto-ignition time in the HCCI combustion will be determined by the initial conditions of the air-to-fuel (AF) mixture at the beginning of the compression stroke and the chemical kinetics of the fuel, making it difficult to control the combustion process and limiting its radius of action (Alkidas, 2007; Yao, Zheng, & Liu, 2009). These problems in HCCI combustion can be minimized with the new Partially Premixed Combustion (PPC) concept that has been evolving greatly over the last few years in CI engines.

In PPC the injection timing is delayed towards the compression stroke and does not match with auto-ignition, generating a combustion process between completely premixed and fully diffusive combustion and controlled through the injection event (J. Benajes, Martín, Novella, & Thein, 2016; Noehre, Andersson, Johansson, & Hultqvist, 2006). The absence of a diffusion flame in PPC provides a reduction in PM emissions, while that NOx formation is limited by the introduction of high levels of EGR providing low combustion temperatures (Okude, Mori, Shiino, & Moriya, 2004; Torregrosa, Broatch, García, & Minico, 2013).

In PPC mode, fuels with a high cetane number (typical of diesel fuels) make it difficult for combustion in properly-phased at high load, the high reactivity of diesel fuel makes it auto-ignite before the AF mixture has the right conditions to begin combustion (SoC) (Bunting, Wildman, Szybist, Lewis, & Storey, 2007; Ickes, Bohac, & Assanis, 2009). On the other hand, the low reactivity of high octane fuels as gasoline allows for the extension of the ignition delay at high loads avoiding the onset of knocking combustion, but at low load can provide instability in combustion and reaching misfire (Hildingsson, Kalghatgi, Tait, Johansson, & Harrison, 2009; Sellnau, Sinnamon, Hoyer, & Husted, 2012; Weall & Collings, 2009). However, different injection system strategies can

solve most of the deficiencies deriving from the chemical kinetics of the fuel and improve the control of the stratification of the charge. The reactivity of the charge can be controlled by injection timing variations, which is the main influence on the degree of stratification (Drews et al., 2010). In this context, it is possible to find different studies in the bibliography that show the relationship between the different strategies of the injection system and PM emission:

The experiments carried out by (Jain, Singh, & Agarwal, 2017) showed an increase in particle number (PN) emissions with SOI delay [from -24 to -12 crank angle (CA) after top dead center (aTDC)], as well as the decrease in injection pressure (from  $8 \times 10^7$  #/cm<sup>3</sup> for 700 bar to  $3 \times 10^7$  #/cm<sup>3</sup> for 1000 bar) in PPC engine. In both cases the authors associate this behavior with a deterioration in the AF mixture preparation thereby facilitating the particles formation.

(Torregrosa et al., 2013) were analyzed different strategies of a pilot injection in diesel engine operating under PPC. Soot emissions increased progressively with the pilot injection timing delay (from -34 to -26 CA aTDC), behavior associated with an increase in percentage of the diffusion combustion due to an insufficient time for AF mixture. However, no significant effect was observed in soot emissions with the pilot injection mass variation.

In the gasoline PPC engine, (Zhang, Wang, Zheng, Reitz, & Yao, 2016) identified two injection timing strategies to maintain a balance between NO<sub>x</sub> emissions (less than 0.4 g / kWh) and smoke emissions (less than 0.1 FSN). One of them was the use of more advanced injection timings (approximately -30 CA aTDC) with relatively low EGR rates (27% to 30%). This is because early injection timing leads to a reduction in the charge reactivity, which reduces the EGR requirement for NO<sub>x</sub> control. The other strategy was the use of more advanced injection timings (from -26 to -18 CA aTDC) and in this case high EGR rates (from 30% to 35%) were necessary to maintain the same NO<sub>x</sub> and smoke values, however under these conditions a slight increase in indicated thermal efficiency was identified.

The main objective of this paper is to analyze experimentally the effects that cause different injection system strategies in PM emissions from a 2-stroke HSDI CI engine using a commercial 95 RON gasoline fuel and operating with the PPC concept. The PN emissions and particle size distribution (PSD) were analyzed in three steady-state operation modes. For each operation mode, three parametric variations of the injection pressure (IP), 2nd and 3rd injection timing were experimentally performed, keeping constant the other parameters that affect the combustion process as the EGR rate.

## **2. Material and methods**

This section contains the main characteristics of the engine, as well as the main properties of the fuel used which are detailed. In addition, detailed descriptions of the different equipment used for pollutants emission measurement and the test methodology are given.

### **2.1. Engine and Fuel Properties**

Experimental activities were performed in the single-cylinder research version of an innovative Renault engine concept, consisting of a two-cylinder 2-stroke HSDI CI engine with scavenge loop.

The combustion chamber has four poppet valves, two intakes and two exhausts, valves with double-overhead camshafts (DOHC) and a staggered roof geometry, specifically designed for masking the flow of air between the intake and exhaust valves, allowing proper scavenging of the burnt gases while keeping short-circuit losses as low as possible. The DOHC are driven by a hydraulic variable valve timing (VVT) system that allows delaying independently intake and exhaust valve timings. Further information on the engine architecture, boost system requirements, combustion chamber geometry and scavenging characteristics can be found in previous publication, presented by (J. Benajes, Molina, Novella, & De Lima, 2014).

The injection system is a common rail HSDI designed for injecting diesel up to a maximum rail pressure of 1800 bar. The injector is equipped with an 8 holes nozzle, with hole diameter of 90 μm and a spray cone angle of 148°. To make possible modifications in the injection timing and the pressure in the rail (represented by the IP), the engine control unit (ECU) was partially opened and the engine setting maps could be recalibrated with the ETAS-INCA software. Detailed specifications of the engine are given in Table 1.

A commercial 95 Research Octane Number (RON) gasoline was used in all the engine tests. The specifications of the fuel properties are provided in Table 2.

**Table 1. 2-stroke HSDI CI engine main characteristics.**

Characteristic	Value
Type	2-Stroke compression ignition
Displacement	365 cm <sup>3</sup> (single cylinder)
Number of valves	4 (2 intake/2 exhaust)
Bore × Stroke	76 mm × 80.5 mm
Connecting rod length	133.75 mm
Compression ratio	17.6:1
Type of scavenge	Poppet valves with scavenge loop
Valvetrain	DOHC with VVT
Fuel injection system	Diesel common rail HSDI
Injector nozzle	8 holes, 90 μm, 148° spray included angle

**Table 2. Gasoline properties.**

Property	Value
Research Octane Number	94.6
H/C ratio	1.76 mol/mol
O/C ratio	0 mol/mol
Oxygen content	<0.17% (m/m)
(A/F) <sub>st</sub> (by mass)	14.37
LHV	42.82 MJ/kg
Density (15 C)	758.1 kg/m <sup>3</sup>
Kinematic viscosity (40 C)	0.44 cSt

## 2.2. Experimental set-up

The engine was connected to an AC electric dynamometer, which allows engine speed and torque control. The test bench was fully equipped with K thermocouples and mean pressure sensors in the exhaust, cooling, intake and lubricating paths. A custom-made low pressure EGR system, designed to provide arbitrary levels of cooled EGR even at very high intake boost pressures, was added. Figure 1 shows the experimental setup for this study, additional information about the instrumentation and accuracy of the measurement equipment are described in detail in (J. Benajes et al., 2014).

Starting with the intake system, an industrial oil-free screw compressor is used to supply pressurized and filtered intake air to the engine. After the air is compressed and filtered, it passes through intercooler system, where the temperature is lower approximately 220 °C to 30 °C, before entering a refrigerant air dryer unit, where the air will be dried to remove water vapor.

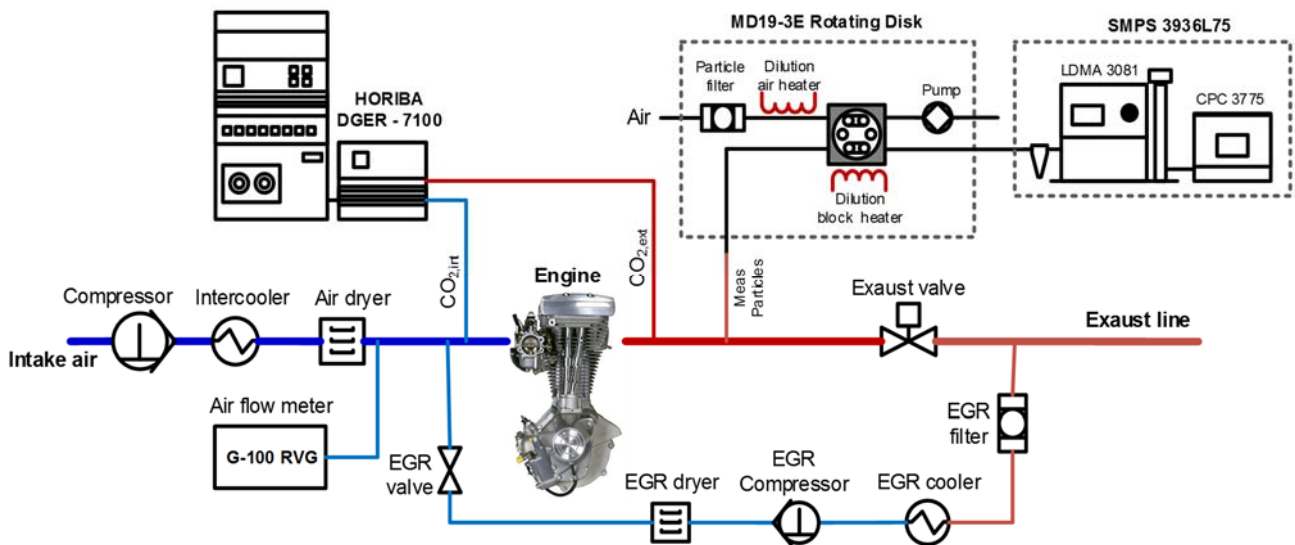


**Figure 1. Experimental set-up for the evaluation of PN emissions and PSD in steady-state operating conditions.**

Once the air is cooled and dehumidified, its volumetric flow rate is measured by a precision Elster G-100 RVG rotary air flow meter, that provides a measurement ranger between 0.05 to 160 m<sup>3</sup>/h with a precision of ±0.1% over the measured value. The flow meter integrates pressure and temperature measurements to calculate the air density, and converter the volumetric flow units into mass flow units.

The fuel mass flow was determined by a Dynamic Fuel Balance AVL-733S, that allows getting a direct measurement in the desired acquisition time, keeping very high accuracy (around 0.12%). The fuel consumption is determined gravimetrically, which means that the density does not have to be determined. The measurement range of the fuel balance is from 0 kg/h to 150 kg/h.

The HORIBA MEXA 7100DEGR which includes a non-dispersive infrared detector (NDIR), was used to measure the carbon dioxide (CO<sub>2</sub>) in the intake and exhaust side. This gas analyzer provides a measurement ranger between 0 to 20 Vol.% with a precision of ±0.1% (full scale).

A single-stage dilution system was coupled with a scanning mobility particle sizer (SMPS) to measure PSD.

The dilution system used in this study was an MD19-3E Rotating Disk, which uses a unique rotating disk method to dilute a sample for particle measurement. Two disks, one with eight and the other with ten cavities allow you to select a dilution ratio from 15:1 to 3000:1. A portion of the raw exhaust is captured by each cavity of the rotating disk and is mixed with preheated and filtered dilution air.

In the MD19-3E RD, the dilution unit and the dilution air may be heated up to selectable temperatures of 200 °C. This method keeps liquids evaporated above their dew point, during and after dilution, and prevents generation of volatile nanoparticles by nucleation. This thermal conditioning of the sample allows for the reduction of the concentration range within the acceptable limits of the particle measuring device and provides accurate information on the concentration of particles generated during the combustion process. The advantages of this dilution system can be analyzed in more detail in previous studies by the authors (Fierz & Burtscher, 2003; Kasper, 2004).

TSI Scanning Particle Sizer (SMPS 3936L75) was used to measure the PSD. This system is equipped with an inertial impactor to remove particles larger than 1 µm; as well as a Long Differential Mobility Analyzer (LDMA 3081) to select the particle size to be measured, with a range from 2.5 to 1000 nm and a Condensation Particle Counter (CPC 3775) to count particles with sizes down to 4 nm.

The operating principle of the SMPS is based on the extraction of an original polydisperse aerosol in different monodisperse fractions by separating the particles according to their size as determined by their electrical mobility inside an electrical field (LDMA). Subsequently, the particles of these monodisperse fractions undergo a saturation process, where the butanol condenses on their surfaces, increasing their size and facilitating the detection and counting in an optical detector that provided the particle number per air volume unit (#/cm<sup>3</sup>) for each particle size (CPC).

To obtain reliable values, the measurement methodology developed by (Desantes, Bermúdez, Pastor, & Fuentes, 2004) was used in this study to dilute the exhaust sample and to measure PSD.

### 2.3. Theoretical tools and calculations method

The EGR rate is calculated from the measured volumetric concentrations of CO<sub>2</sub>, as shown in Equation (1). The CO<sub>2,int</sub> is the Vol.% of CO<sub>2</sub> measured at the intake manifold being CO<sub>2,exh</sub> the Vol.% of CO<sub>2</sub> taken at exhaust manifold. Atmospheric carbon dioxide was considered as CO<sub>2,atm</sub>.

$$EGR = \frac{CO_{2,int} - CO_{2,atm}}{CO_{2,exh} - CO_{2,atm}} \cdot 100 \quad (1)$$

To obtain accurate values of PN concentration; the PSD may be decomposed by Equation (2), according to (Seinfeld & Pandis, 2006). It establishes that total particle size distribution is the sum of two particle concentrations modes (nucleation-mode and accumulation-mode), assuming the log-normal size distribution function:

$$\frac{dN_i}{d \log dp_i} = \frac{1-x}{\sqrt{2\pi} \log \sigma_{g1}} \cdot e^{-\frac{\log^2\left(\frac{dp_1}{dp_{g1}}\right)}{2 \log^2 \sigma_{g1}}} + \frac{1-x}{\sqrt{2\pi} \log \sigma_{g2}} \cdot e^{-\frac{\log^2\left(\frac{dp_2}{dp_{g2}}\right)}{2 \log^2 \sigma_{g2}}} \quad (2)$$

Where  $x$  is the ratio of the total concentrations number of two distributions,  $d_{p1}$ ,  $d_{p2}$ ,  $d_{pg1}$ ,  $d_{pg2}$ ,  $\sigma_1$  and  $\sigma_2$  are the geometric mean diameters, median diameters, and geometric standard deviations of each peak, and  $N_i$  is the particle concentration of particle size  $d_{pi}$ . The fit was achieved by minimizing the mean square error function by means of the Nelder–Mead simplex method.

To calculate the total particle number concentration ( $dN$ ) and geometric mean diameter (GMD), the Equations (3) and (4) were used for each mode:

$$dN = \sum_{dp(low)}^{dp(up)} dN_i \quad (3)$$

$$GMD = \frac{\sum_{dp(low)}^{dp(up)} dN_i \ln dp_i}{dN} \quad (4)$$

In order to convert the numerical concentration to mass concentration ( $dM$ ) was used Equation (5), experimentally determined using the particle density on a GDI engine (Symonds, Price, Williams, & Stone, 2008).

$$dM_i = 1.72 \cdot 10^{-24} \cdot dp_i^{2.65} \quad (5)$$

From the density, the mass to diameter relationship was determined, with a power law fit yielding a fractal dimension of 2.65. The fractal dimension gives an indication of how completely a particle appears to fill space; if the particles were spherical they would have a fractal dimension of 3 (Chen, Stone, & Richardson, 2012).

Finally, the most relevant global combustion parameters like indicated mean effective pressure (IMEP), peak cylinder pressure ( $P_{max}$ ), pressure gradient ( $dP/d\alpha$ ) are directly derived from the analysis of the cylinder pressure signal; while the SoC, main combustion angles [(crank angle for 10% of fuel burnt (CA10) and crank angle for 50% of fuel burnt (CA50)], ignition delay and mixing times are obtained from the calculated rate of heat release (RoHR). A dedicated 0-dimensional combustion analysis software (CALMEC) (M. Lapuerta, Armas, & Hernandez, 1999; Payri, Molina, Martín, & Armas, 2006) is used to resolve the first law of thermodynamics; taking the cylinder as a control volume independently from the local conditions inside the combustion chamber; and obtain the instantaneous evolution of the energy released by the progress of combustion from measured cylinder pressure signal.

#### 2.4. Test schedule

In this study, a parametric study was carried out based on the independent modification of three injection system parameters: the IP, 2nd injection timing and 3rd injection timing, from a reference point, which corresponds to nominal engine configuration in steady-state operation mode. The main characteristics of these operating points are shown in Table 3, where the reference point settings are indicated in bold. The operation modes are defined by their engine speed and IMEP, and are denoted as A2000, B2000 and C2500.

A multiple injection strategy (triple or double injection) was used in all experiments presented in this research, with a fixed fuel mass flow which provided the required IMEP target at the reference case at each operation mode. The air management was adjusted through the following parameters: the intake pressure, the EGR rate, the valve overlap (OLAP) and the differential pressure between intake and exhaust ( $\Delta P$ ). For this purpose, a second-order mathematical model was employed to identify the appropriate values of these parameters in terms of oxygen concentration and mean gas temperature at intake valve closing to assure proper ignition around TDC when operating with the PPC concept (Jesus Benajes, Novella, De Lima, & Tribotte, 2015).

The injection timing shown in the paper (see Table 3 as an example), correspond to the start of energizing (SoE) of the injector instead of the actual start of injection, which takes place a few degrees ( $\approx 150 \mu s$ , i.e. 1.5 to 2 CA) after the SoE due to the hydraulic delay affecting the needle lift.

The SoE1 was not analyzed due to its reduced impact on the exhaust emissions, only a slight increase in the HC emissions to medium and high load was observed in previous studies by (J. Benajes, Novella, De Lima, & Thein, 2017). The main application of this early injection is mainly to provide the required amount of fuel to sustain the demanded IMEP, avoiding the injection of this fuel in either of the other events where it could interfere with the combustion conditions and pollutant formation.

**Table 3. Experimental plan for the parametric study.**

Point	Speed [rpm]	IMEP [bar]	IP [bar]	SoE2 [CA aTDC]	SoE3 [CA aTDC]	SoE1 [CA aTDC]	OLAP [CA]	$\Delta P$ [mbar]	EGR [%]	$M_{fuel}$ [mg/st]	%Fuel [%]
<b>A2000</b>	<b>2000</b>	<b>3.5</b>	<b>400</b>	-44	<b>-10</b>	-	<b>66.4</b>	<b>250</b>	<b>26</b>	<b>7.4</b>	<b>-176/24</b>
			500	<b>-42</b>	-8						
			600	-40	-6						
<b>B2000</b>	<b>2000</b>	<b>5.5</b>	<b>400</b>	-44	<b>-10</b>	<b>-60</b>	<b>63.4</b>	<b>450</b>	<b>32</b>	<b>11.5</b>	<b>18/62/20</b>
			<b>600</b>	<b>-42</b>	-8						
			800	-40	-6						
<b>C2500</b>	<b>2500</b>	<b>5.5</b>	<b>500</b>	-48	-14	<b>-60</b>	<b>65.4</b>	<b>475</b>	<b>29</b>	<b>11.8</b>	<b>18/65/17</b>
			<b>600</b>	<b>-46</b>	-12						
			700	-44	<b>-10</b>						

As part of the research process of PPC concept in this engine, in previous works were analyzed other operation modes, at low-to-medium engine speed (1200/1500 rpm) and almost the full load range (3.1/5.5/10.4 bar IMEP) (J. Benajes et al., 2016; Jesus Benajes, Martin, Novella, & De Lima, 2014). Here the focus is new operating conditions at high speed (2000/2500 rpm) and other loads (3.5/5.5 bar IMEP). So, it can be said that this is the main reason why these operation modes were chosen.

### 2.5. Methodology for testing steady-state operating points

In this experimental study, a strict measurement methodology was established as shown in Figure 2. This protocol aims to control all aspects that could introduce variability in the measurements and to reduce the experimentation time as much as possible. The methodology is described below:

- Once the specifications of the measurement point (IMEP, engine speed and injection system parameters) are defined, a stabilization time of 15 minutes is considered before the first measurement.
- After this stabilization time, three different parameters (EGR rate, air mass flow and fuel mass flow) are measured simultaneously and this measurement is repeated twice more, the values of these three measurements should be similar and are used to identify any variation in the steady-state of the point.
- In addition, three consecutive PSD measurements with an interval of 5 min between them were carried out and, with this, a most representative experimental mean value was obtained.
- Finally, when the third PSD measurement is taken, the specifications of the next measurement point are defined, and the above procedure is repeated.

This procedure allowed data to generate results variability analysis from measurements and to obtain the mean value and deviation of each variable.

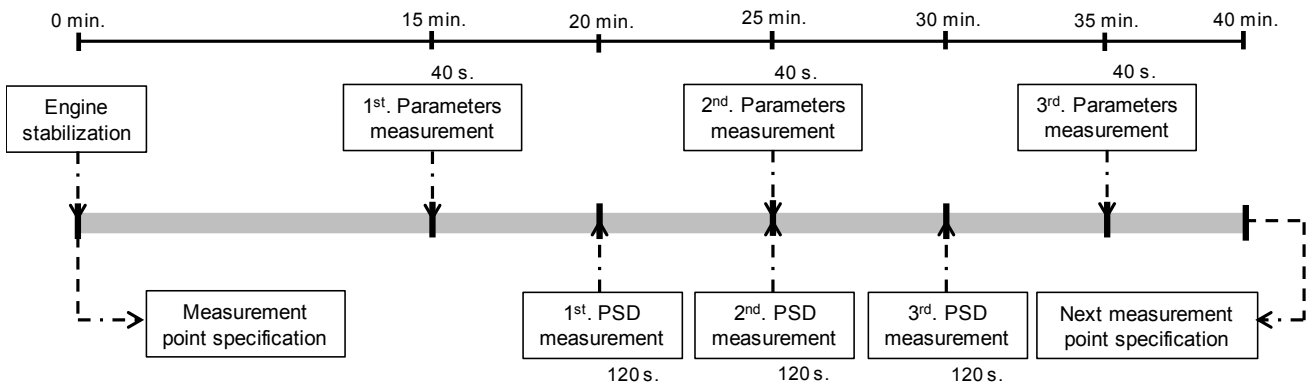


**Figure 2. Methodology applied for PSD and different parameters (EGR rate, air mass and fuel mass) measurement at each steady-state operating point.**

### 3. Results and discussion

The influence of different injection system strategies on PM emissions will be analyzed in this section.

#### 3.1. Soot formation mechanism

It is necessary to state how soot particles are formed inside the cylinder during the combustion process due to the fact -that the injection system parameters variation has strong effects on combustion process.

It is well known that soot is mainly carbon originated from high combustion temperature and it is produced as an intermediate step between the fuel evaporation and fuel dehydrogenation (Mueller, Blanquart, & Pitsch, 2009). The evolution of molecules from vapor-phase or liquid-phase to solid soot particles includes phenomena such as described in terms of three steps: nucleation, growth and oxidation (Clague, Donnet, Wang, & Peng, 1999). The process occurs under fuel-rich conditions, in both premixed and non-premixed combustion, where the local equivalent ratio is more than one (Bonatesta, Chiappetta, & La Rocca, 2014).

The nucleation process takes place under high temperature conditions, between 1000 and 2800 K, where the fuel undergoes the pyrolysis phenomenon and its molecular structure is altered and partially oxidized, mainly generating compounds such as acetylene ( $C_2H_2$ ), ethylene ( $C_2H_4$ ) and methane ( $CH_4$ ) (Haynes & Wagner, 1981). From this point, the rings of aromatic compounds begin to form, due to the attack of  $C_2H_2$  on the  $n-C_4H_3$  radicals (in high temperature processes) or on the radicals  $n-C_4H_5$  (in low temperature processes). After this process, the aromatic rings undergo a transformation mechanism, known as hydrogen abstraction-acetylene addition (HACA), which promotes molecular growth of polycyclic aromatic hydrocarbons (PAH) (Frenklach & Wang, 1994; Park, Wang, Chung, & Sarathy, 2017). To finish the nucleation process, the high supersaturation of the macromolecular precursors (PAH) produces a series of condensation reactions that yield primary soot particles in liquid phase. This phenomena gives rise to a large number of primary soot particles with a diameter of less than 2 nm and with an insignificant soot load (Amann & Siegl, 1981; Bockhorn & Schäfer, 1994).

In the final stage of soot formation, surface growth is a predominant process which occurs by the addition of mass on the nucleate soot particle surface and leads to an increase in the soot mass. During surface growing, active reactant is portion of primary soot particle accepts the gas-phase of acetylene hydrocarbons. This mechanism (for surface growing) continues when the primary particles are moved to less active cold areas, where the hydrocarbon concentration is less than the limit of soot inception rate (Mosbach et al., 2009). The coagulation is another mechanism that occurs in this phase, which is characterized by the collision of the nuclei, fusing with each other, giving rise to aggregates in the form of chain (secondary particles), with a consequent increase in size, the particle number present is reduced in this process.

Unlike the phenomenon of surface growth, which occurs in a defined phase, the oxidation phenomenon takes place during all stages of soot formation. It has been experimentally proven that oxidation occurs through an attack on precursors, nuclei and particles of oxidizing species such as  $O_2$ ,  $O$ ,  $OH$ ,  $CO_2$ ,  $H_2O$  (Stanmore, Brilhac, & Gilot, 2001). The vast majority of soot formed is completely oxidized during the combustion process (Velji et al., 2010).

#### 3.2. Particle Size Distribution

The PSD is a way of representing the PM emissions, and is represented by a bimodal structure (nucleation-mode and accumulation-mode). The nucleation-mode represents the particles with sizes of less than 50 nm in diameter, although some authors define this limit as 30 nm (Kumar, Fennell, & Britter, 2008; Magín Lapuerta, Armas, & Gómez, 2003), the particles belonging to this mode are principally formed by volatile organic and sulfur compounds, and they are believed to form during cooling and dilution processes (Charron & Harrison, 2003; RÖnkkÖ et al., 2007). The accumulation-mode is formed for particles between 30 nm to 1  $\mu m$  and its chemical composition is of agglomerates of soot with hydrocarbons absorbed on the surface (David B. Kittelson, 1998; Wang et al., 2016).

In general, both modes were observed in this work. For the nucleation-mode, particles of less than 30 nm and for the accumulation-mode, the particle range was between 30 and 237 nm.

#### 3.3. Influence of injection pressure

The results of the experimental analysis of the influence of IP on PN emissions are shown in this section. Lognormal PSD obtained by averaging three SMPS consecutive scans are presented in number and mass. Mass concentrations were calculated using Equation 6 defined in section 2.3. Also, particle composition analysis separating nucleation-mode, accumulation-mode and total particles emitted is shown.

Due to the small particle size of the nucleation-mode, these have very little mass, so their effect on particle mass distribution is insignificant. By contrast, the much larger particle size of the accumulation-mode makes this mode particularly noticeable with respect to the nucleation-mode when representing the particle mass distribution.

The IP increase improves the fuel atomization process and increase the amount of air entrained into the spray before ignition, reducing locally fuel-rich zones. Additionally, in PPC concept this behavior shifts the local equivalence ratio distribution towards leaner conditions, and consequently the SoC and its phase (represented by the CA50) are delayed, decreasing the RoHR peak as shown in Figure 3. This has been explained by CFD calculation, and presented in (J. Benajes et al., 2017; J. Benajes, Novella, De Lima, & Tribotte, 2015), showing how the homogeneity of the mixture (and so the local richness) influences its reactivity and hence determines the combustion timing.

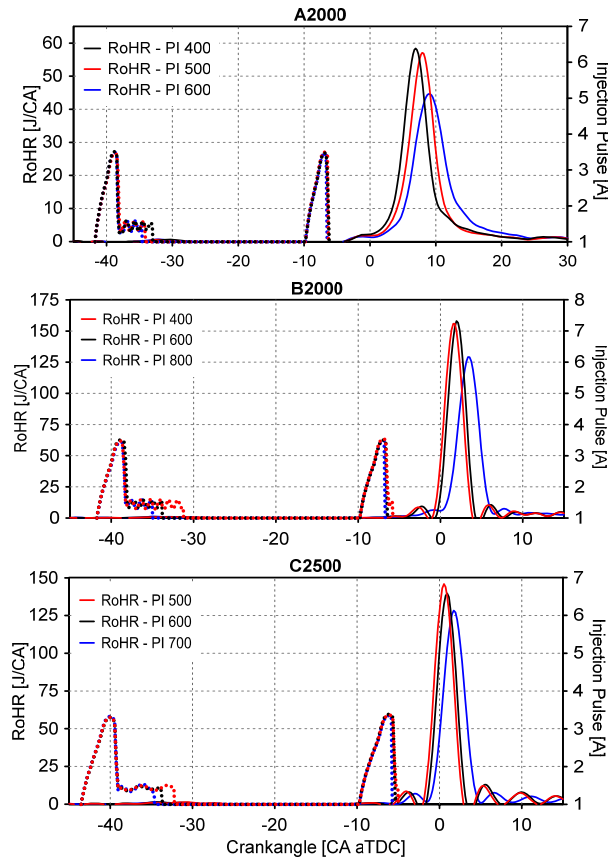


Figure 3. Effect of IP over RoHR at each operation mode.

Figure 4 shows the effect of IP variation over the SoC (represented by CA10), CA50, the maximum pressure gradient ( $dP/d\alpha_{max}$ ) and peak cylinder pressure ( $P_{max}$ ), for the three operation modes. In general terms, as expected from the trends already observed in RoHR, the advance of CA10 and CA50 provides an increase in the values of  $dP/d\alpha_{max}$  and  $P_{max}$  cause the trends to generate a constant volume combustion. As a result of the high  $P_{max}$ , the local temperature of the reaction zones increases.

Therefore, considering that the first step for particle formation occurs under fuel-rich zones and depends on the high temperatures, as well as IP decreasing caused by an increase in the combustion temperature and rich local equivalence ratio zones, then the formation process of nuclei-precursor particles is facilitated and, consequently, the total PN emissions increase as the IP decreases as shown in Figures 5A.1, 5B.1 and 5C.1.

For the B2000 operation mode the total particle concentration increased up to 32% (from  $2.54 \times 10^7 \text{ \#/cm}^3$  for 800 bar to  $3.36 \times 10^7 \text{ \#/cm}^3$  for 400 bar); and for the C2500 operation mode the increase was 102% (from  $5.17 \times 10^7 \text{ \#/cm}^3$  for 700 bar to  $1.05 \times 10^8 \text{ \#/cm}^3$  for 500 bar of the IP). In both operation modes, it is observed how the PSDs are shifted to larger sizes with the IP decrease, increasing the particle concentration of the accumulation-mode (Figures 5B and 5C). The effects of IP decrease in the increment of the number of nuclei-precursor that make up the soot particles could explain the above result. With more nuclei particles, the surface growth and coagulation rates increase (Maricq, Podsiadlik, Brehob, & Haghgoie, 1999; Saxena & Maurya, 2017; Sgro et al., 2012), thus leading to the increase in size and particle number when the IP decreases.

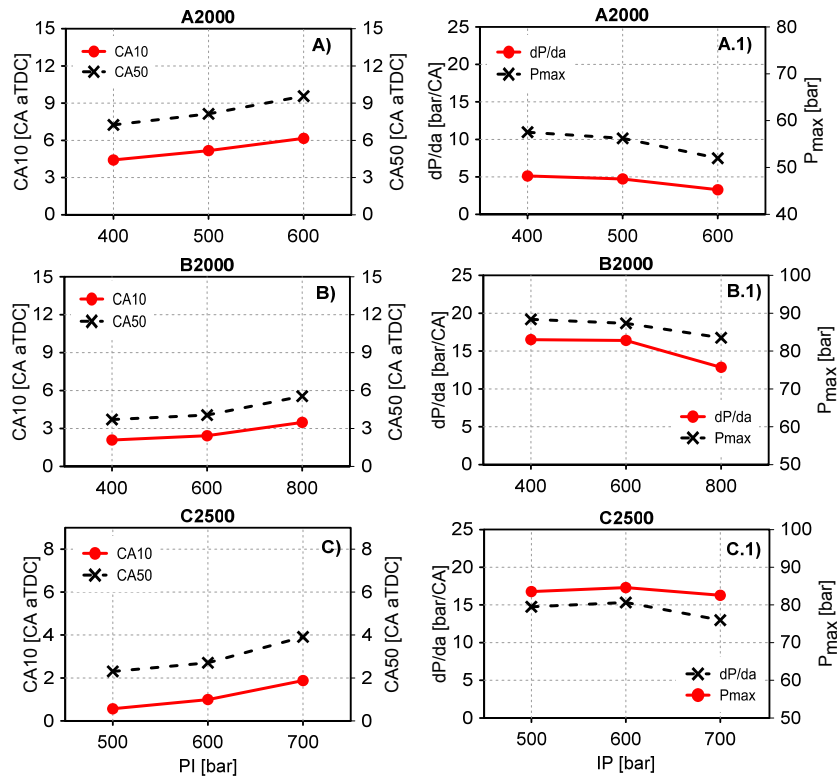


Figure 4. Effect of IP over the  $dP/da_{max}$ ,  $P_{max}$ , CA10 and CA50 at each operation mode.

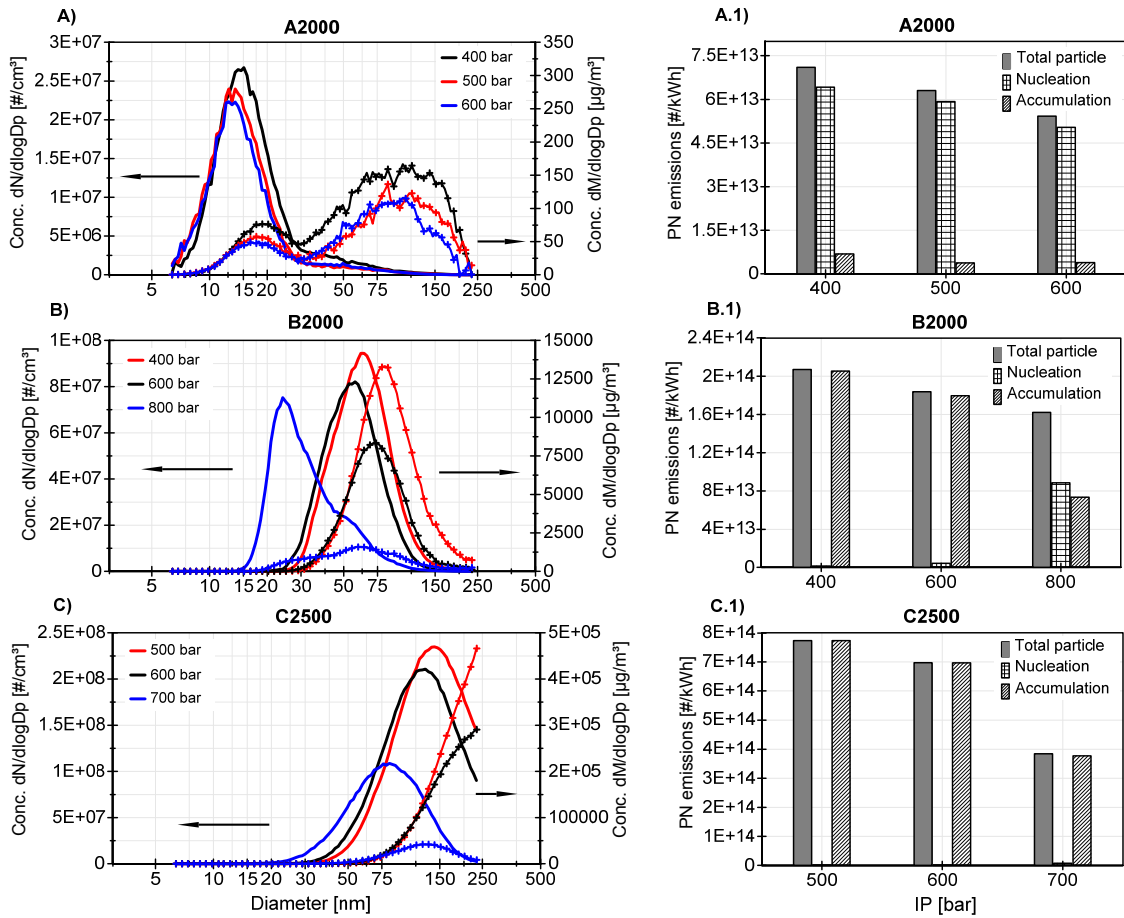


Figure 5. Influence of IP over particle size distributions and PN emissions at each operation mode.

In A2000 operation mode the total particle concentration increased by 8% (from  $7,69 \times 10^6 \text{ \#/cm}^3$  for 700 bar to  $8.34 \times 10^6 \text{ \#/cm}^3$  for 500 bar). As shown in Figure 5A, the PSDs is made up of a high nucleation-mode and a very low accumulation-mode. The changes of the accumulation-mode can be observed in the particle mass scale, as the particle number is so low that the variation cannot be clearly observed in the number scale. In the nucleation-mode, a slight increase in PN emissions was observed with the IP decrease, without significant shifts of the PSDs to larger sizes. Due to the low PN emission values and the small variation of the PSDs it is possible to conclude that the variation of the IP does not have a significant effect on the particulate emissions in this operation mode.

The high nucleation mode that appears in the A2000 operating mode and 700 bar in the B2000 operating mode may be associated with the low amount of carbonaceous particle generated under these conditions. In this case, the nucleation-mode particles are favored by the small number of the accumulation-mode particles, due to the low adsorption of volatiles that can take place on the surface of the carbonaceous particle under these conditions (Desantes, Bermúdez, García, & Fuentes, 2005; D.B. Kittelson, Watts, & Johnson, 2006).

To provide a better understanding of the effect of IP on PSD, Figure 6 shows the calculated GMD for each operation mode. This value points out the overall value of PSD considering both particle concentration for each diameter and total particle concentration (Equation 5).

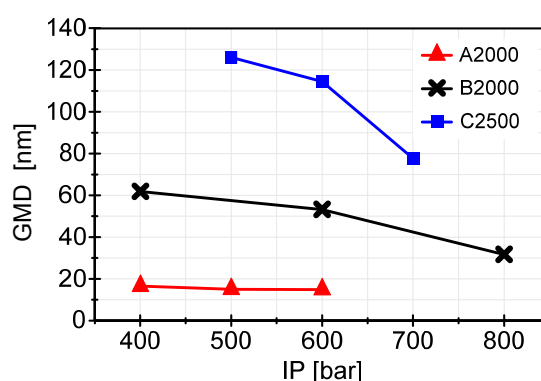


Figure 4. Effect of IP over GMD at each operation mode.

In A2000 operation mode no observed significant variations in the GMD values for different IPs, this shows that the particle concentration was kept in the nucleation-mode without significant alterations of the PSD width. In B2000 and C2500 operation modes a reduction of the GMDs with the IP increase was observed, showing a relation between the GMD values and the PN emissions. For the B2000 operation mode the GMDs varied between 30 and 62 nm, which confirms that there was particle concentration in nucleation-mode and accumulation-mode. As such, for the C2500 operation mode there was an increase of the GMD values, from 77 nm. This result indicates that the particle concentration was exclusively in the accumulation-mode.

### 3.4. Influence of 2nd injection timing

In PPC, the range of SoE2 is limited by poor combustion stability and misfire in the case of very advanced SoE2s, and by the onset of knocking combustion in the case of very delayed SoE2s (J. Benajes et al., 2015; Jesus Benajes et al., 2015). However, little variations of the SoE2 can be performed, without altering the IMEP values in order to study its effects on particle emissions.

Figures 7A, 7B and 7C show the effect of SoE2 on the SoC and the combustion phase for the three operation modes. The SoE2 delay increases the ignition delay and consequently decreases the  $dP/d\alpha_{max}$  and  $P_{max}$  values as shown in Figure 7A.1, 7B.2 and 7C.1.

Under these conditions the time available for the AF mixture preparation is not significantly affected, because when the SoE2 is advanced the SoC is also delayed, a behavior that reduces the development of the rich local equivalence ratio zones and the particle emission variations. However, in Figures 8A.1, 8B.1 and 8C.1 it is possible to observe a slight decrease in PN emissions in the three operation modes with the SoE2 advance. In A2000 operation mode there was a decrease around 8% ( $1.07 \times 10^7 \text{ \#/cm}^3$  to  $9.36 \times 10^6 \text{ \#/cm}^3$ ), in B2000 operation mode this increase was 10% ( $2.92 \times 10^7 \text{ \#/cm}^3$  to  $2.63 \times 10^7 \text{ \#/cm}^3$ ), and in C2500 operation mode was 7% ( $9.22 \times 10^7 \text{ \#/cm}^3$  to  $8.58 \times 10^7 \text{ \#/cm}^3$ ). The previous result is related to the extended ignition delay and, therefore, increased the time available for the AF mixture preparation for the 3rd injection timing. This late injection has a much greater influence on PN emissions, as will be seen in the next section.

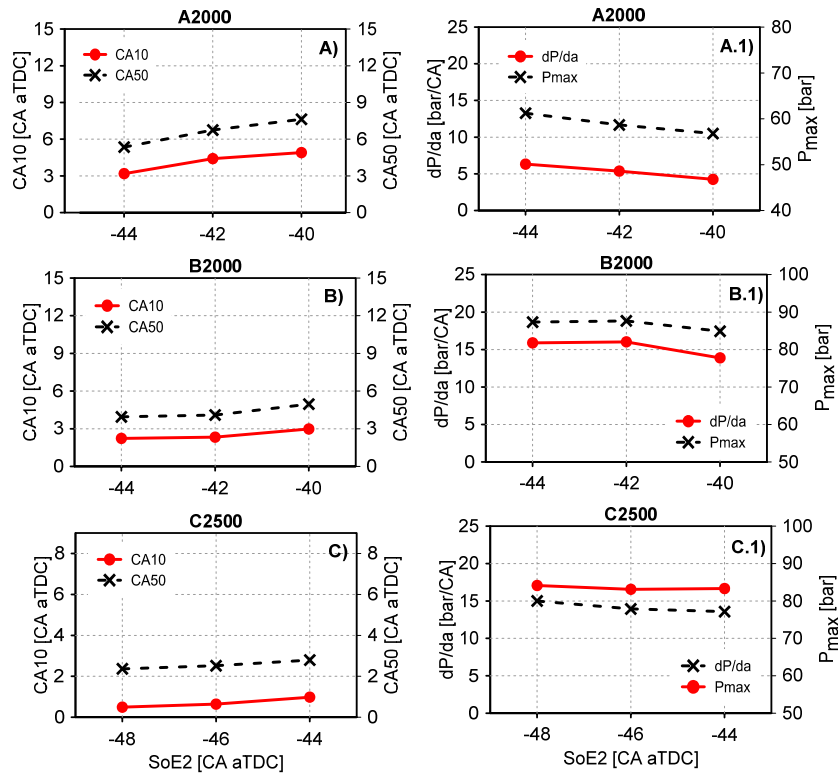


Figure 7. Effect of SoE2 over the  $dP/da_{max}$ ,  $P_{max}$ , CA10 and CA50 at each operation mode.

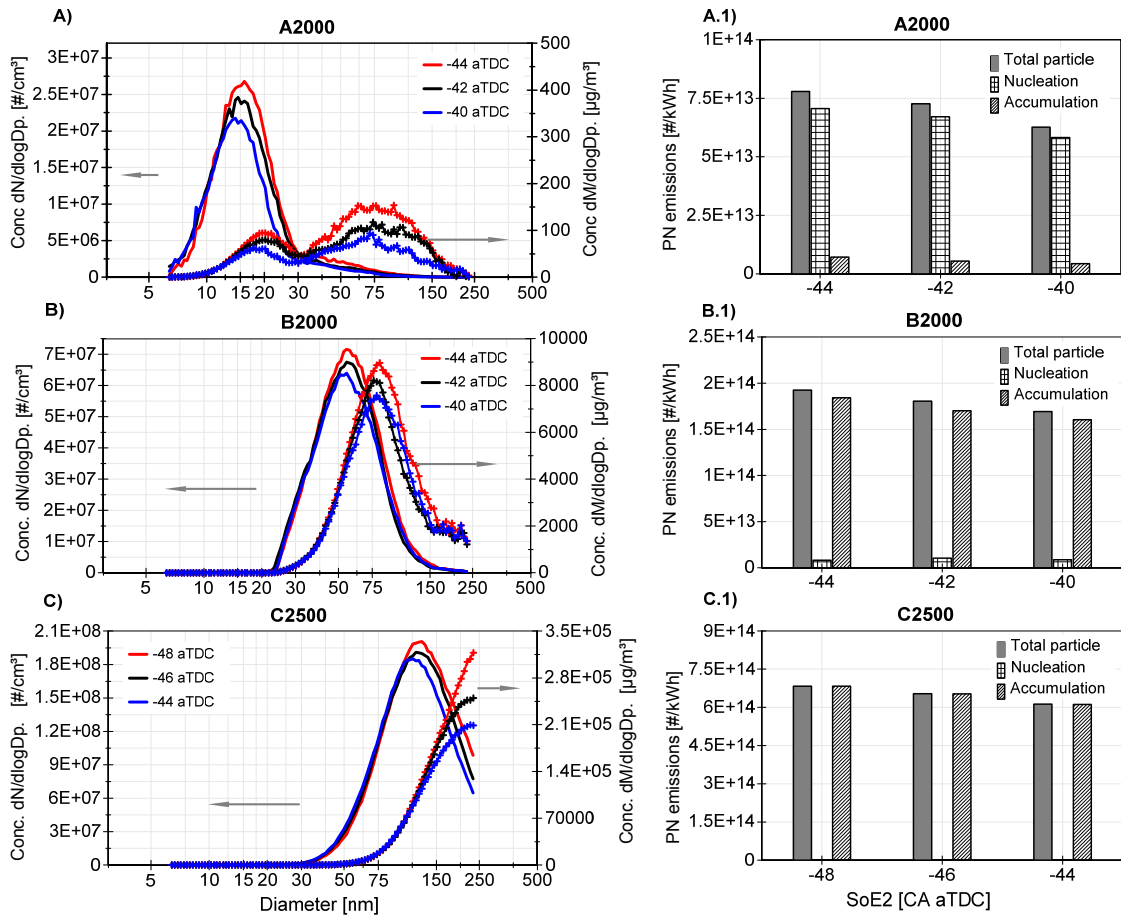


Figure 8. Influence of SoE2 over particle size distributions and PN emissions at each operation mode.

Figures 8A, 8B and 8C show how the PSDs does not shift with the SoE2 variation in any of the three operation modes, this can be confirmed in the GMD constant values for each operation mode in Figure 9. However, an increase in the PN emissions with the SoE2 delay was observed, which means that the slight increase in the primary particle number are not enough to favor the particles growth.

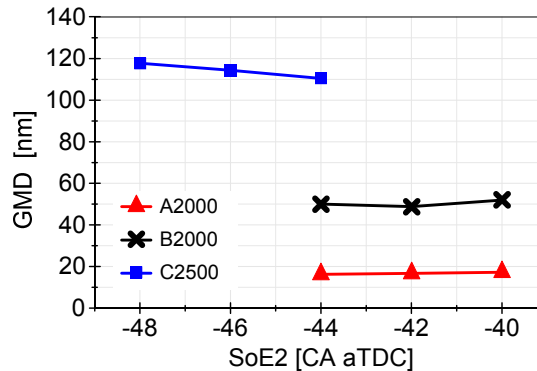


Figure 5. Effect of SoE2 over GMD at each operation mode.

The small variations of the PN emissions for the different SoE2s in each operation mode, as shown in Figure 8, allow for the comparison of the behavior of the particle emissions between the operation modes. In this case, the load and engine speed would be responsible for the changes in PN emissions values.

It is also possible to observe how PSDs are in the nucleation-mode for the operation mode A2000 (3.5 bar of IMEP), nonetheless with an increase of the load to 5.5 bar (B2000 operation mode) the PSDs shifted to an accumulation-mode (Figure 8A and 8B). Specifically, when both reference points were compared, the increase in PN emissions was 196% (from  $6.25 \times 10^{13}$  #/kWh for the A2000 reference point to  $1.84 \times 10^{14}$  #/ kWh for the B2000 reference point), a result that may be associated with the increase in the fuel mass (from 7.3 mg/st for A2000 operation mode to 11.5 mg/st for B2000 operation mode) which as a consequence may cause a less efficient process of AF mixture preparation (Arsie, Di Iorio, & Vaccaro, 2013; Kalghatgi, Risberg, & Angstrom, 2007).

Finally, a shift of the PSDs from B2000 to larger sizes (mode of operation C2500) was observed, with a considerable increase in particle emission, which was of 255% (from  $1.84 \times 10^{14}$  #/kWh for the A2000 reference point to  $6.53 \times 10^{14}$  #/ kWh for the B2000 reference point). In this case, although there are no significant variations in the fuel mass, the increase of the engine speed (2000 rpm to 2500 rpm) provides a shorter time for the AF mixture preparation and for the particle oxidation, resulting in an increase in PN emissions as shown in Figure 8B.1 and 8C.1.

### 3.5. Influence of 3rd injection timing

The effect of the SoE3 can be considered as complementary to those of the IP, as SoE3 delay has similar impacts on combustion and PN emissions as when the IP decreases. The SoE3 delay decreases ignition delay and the time for the AF mixture, increasing the rich local equivalence ratio zones and the reactivity of the global mixture. Consequently, SoC and CA50 advance, while combustion is faster with a higher  $P_{max}$ , as shown in Figure 10 in the three operation modes.

In terms of PN emissions, Figures 11A.1, 11B.1 and 11C.1 show how SoE3 delay increases the particle formation in the three operation modes. This may be related to the short ignition delay and the available mixing time and, as a result, the combustion of the fuel injected in this 3rd injection shifts from a highly premixed process to a mixing-controlled process, recovering the characteristic of the CDC concept, with a critical impact on particle emissions. When comparing the PN emissions for the different SoE3 the increase was 279% for A2000 (from  $8.82 \times 10^6$  #/cm<sup>3</sup> for -10 CA aTDC to  $3.34 \times 10^7$  #/cm<sup>3</sup> for -6 CA aTDC), 181% for B2000 (from  $3.06 \times 10^7$  #/cm<sup>3</sup> for -10 CA aTDC to  $8.59 \times 10^7$  #/cm<sup>3</sup> for -6 CA aTDC) and 61% for C2500 (from  $6.17 \times 10^7$  #/cm<sup>3</sup> for -14 CA aTDC to  $9.92 \times 10^7$  #/cm<sup>3</sup> for -10 CA aTDC). The increase of the values of the GMDs with the SoE3 delay for the three operation modes as shown in Figure 12 and the previous behavior is confirmed.

Figures 11A, 11B and 11C show a considerable shifting the PSDs to larger sizes, increasing the concentration of accumulation-mode with the SoE3 delay. This behavior may be associated with a considerable favoring of surface growth and coagulation rate, provided by the significant increase of particle precursors (nuclei particles) which are formed when the partially premixed flame propagates through these locally fuel rich zones.

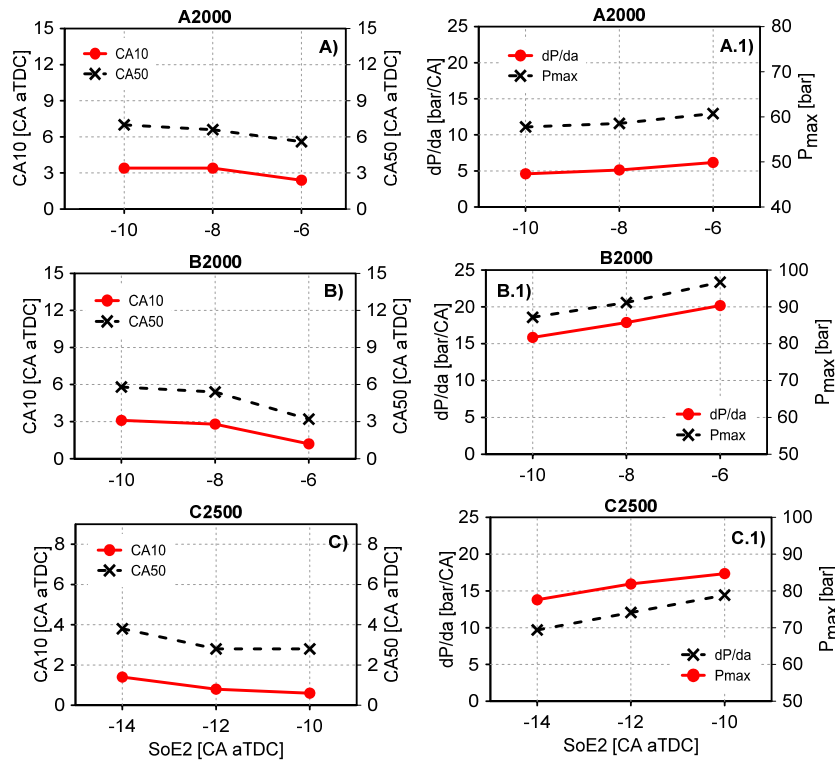


Figure 10. Effect of SoE3 over the  $dP/d\alpha_{max}$ ,  $P_{max}$ , CA10 and CA50 at each operation mode.

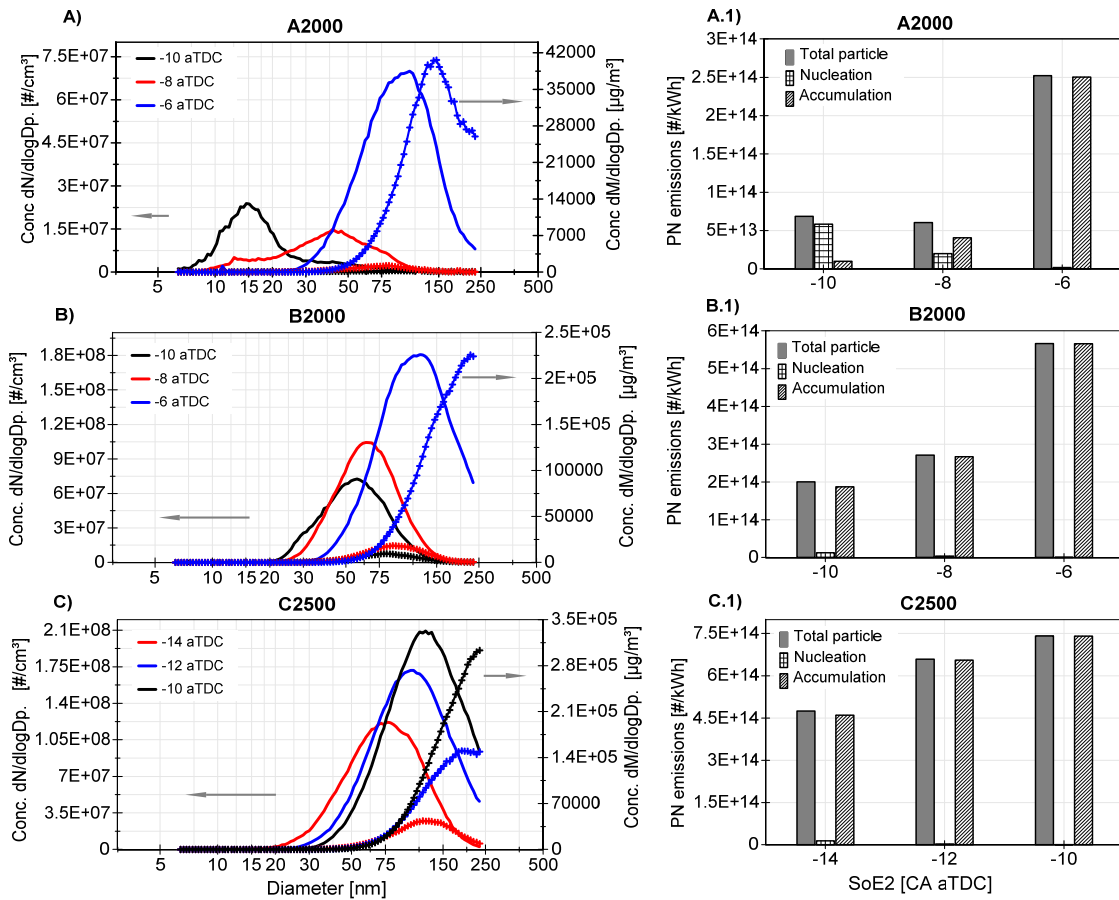


Figure 11. Influence of SoE3 over particle size distributions and PN emissions at each operation mode

Specifically, in A2000 operation mode it is possible to observe how the particle concentration of the nucleation-mode decreases as the particle concentration of the accumulation-mode increases, confirming the hypothesis described in section 3.2, which explains that the accumulation particles reduce nucleation particles.

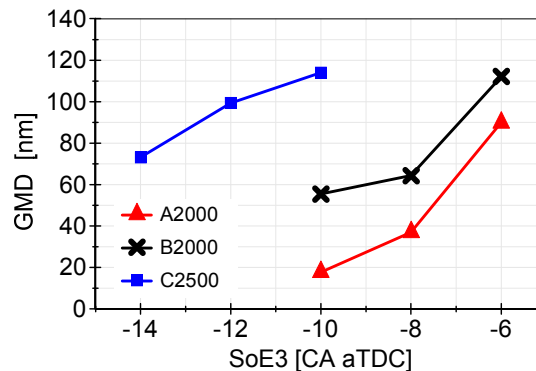


Figure 6. Effect of SoE3 over GMD at each operation mode.

## 4. Conclusions

This paper presented an experimental study in a two-cylinder 2-stroke HSDI CI engine using a RON 95 gasoline and operating with PPC concept. The effects of injection pressure, 2nd injection and 3rd injection timing on reactivity of the AF mixture and available mixing time, its consequent impact on PN emissions, particle size distribution and GMD was experimentally investigated in three steady-state operation modes.

The IP decrease and the 3rd injection timing delay affect the global mixture reactivity, advancing the combustion phase and increasing the pressure gradient. Both factors reduce the AF mixture time available, increasing fuel-rich zones and combustion temperatures. Under these conditions the soot particle formation process is facilitated and the PN emissions increase, a behavior that was more prominent in the 3rd injection timing.

Additionally, the 3rd injection timing delay and the IP decrease provided a progressive shifted of the numeric and mass distribution towards larger sizes, increasing the particle concentration of accumulation-mode and the GMD values. However, the injection pressure variation and specifically for the more advanced 3rd injection timing in the A2000 operation mode where the PN emissions were in much lower quantities, a size distribution was dominated by the nucleation-mode with a very low accumulation-mode concentration and without significant variations of the GMD values. This last behavior supports the hypothesis that a low particle number of the accumulation-mode favors the formation of nucleation-mode particles, due to the low absorption of volatiles that can take place on the surface of the carbonaceous particle.

The 2nd injection timing delay increased the ignition delay, so the time available for the AF mixture preparation was not significantly affected in any of the three operation modes. Under these conditions, there were no significant changes in particulate emissions alone, a slight decrease in PN emissions when the SoE2 was delayed, due to a slight increase in AF mixture time for the 3rd injection timing.

It was also found that engine speed and load conditions greatly influenced particle size distributions and PN emissions. With increasing load, PN emissions increased by shifting the particle concentration from the nucleation mode to the accumulation mode, behavior that could be associated with the increase of the fuel mass. This shift of the size distribution and the PN emissions increase was made worse with the engine speed increase, under these conditions the reduction of the time available for the AF mixture and for the particle oxidation could be the main causes.

This study demonstrates that an appropriate injection strategy in the new PPC concept is not only important for proper engine performance, but also has a significant impact on PM emissions. A very important aspect nowadays due to the new and demanding emission regulations.

## Acknowledgments

This work was partly funded by the Generalitat Valenciana – Spain, project PROMETEOII/2014/043. The authors kindly recognize the technical support provided by Mr. Pascal Tribotté from RENAULT SAS – France in the frame of the DREAM-DELTA-68530-13-3205 Project.

## 5. References

- Alkidas, A. C. (2007). Combustion advancements in gasoline engines. *Energy Conversion and Management*, 48(11), 2751–2761. <https://doi.org/10.1016/j.enconman.2007.07.027>
- Amann, C. A., & Siegl, D. C. (1981). Diesel Particulates—What They Are and Why. *Aerosol Science and Technology*, 1(1), 73–101. <https://doi.org/10.1080/02786828208958580>
- Arsie, I., Di Iorio, S., & Vaccaro, S. (2013). Experimental investigation of the effects of AFR, spark advance and EGR on nanoparticle emissions in a PFI SI engine. *Journal of Aerosol Science*, 64, 1–10. <https://doi.org/10.1016/j.jaerosci.2013.05.005>
- Benajes, J., Martín, J., Novella, R., & De Lima, D. (2014). Analysis of the Load Effect on the Partially Premixed Combustion Concept in a 2-Stroke HSDI Diesel Engine Fueled with Conventional Gasoline. In *SAE Technical Paper. 2014-01-1291*. <https://doi.org/10.4271/2014-01-1291>
- Benajes, J., Martín, J., Novella, R., & Thein, K. (2016). Understanding the performance of the multiple injection gasoline partially premixed combustion concept implemented in a 2-Stroke high speed direct injection compression ignition engine. *Applied Energy*, 161, 465–475. <https://doi.org/10.1016/j.apenergy.2015.10.034>
- Benajes, J., Molina, S., Novella, R., & De Lima, D. (2014). Implementation of the Partially Premixed Combustion concept in a 2-stroke HSDI diesel engine fueled with gasoline. *Applied Energy*, 122, 94–111. <https://doi.org/10.1016/j.apenergy.2014.02.013>
- Benajes, J., Novella, R., De Lima, D., & Thein, K. (2017). Impact of injection settings operating with the gasoline Partially Premixed Combustion concept in a 2-stroke HSDI compression ignition engine. *Applied Energy*, 193, 515–530. <https://doi.org/10.1016/j.apenergy.2017.02.044>
- Benajes, J., Novella, R., De Lima, D., & Tribotte, P. (2015). Analysis of combustion concepts in a newly designed two-stroke high-speed direct injection compression ignition engine. *International Journal of Engine Research*, 16(1), 52–67. <https://doi.org/10.1177/1468087414562867>
- Benajes, J., Novella, R., De Lima, D., & Tribotte, P. (2015). Investigation on Multiple Injection Strategies for Gasoline PPC Operation in a Newly Designed 2-Stroke HSDI Compression Ignition Engine. *SAE International Journal of Engines*, 8(2), 758–774. <https://doi.org/10.4271/2015-01-0830>
- Bockhorn, H., & Schäfer, T. (1994). Growth of Soot Particles in Premixed Flames by Surface Reactions (pp. 253–274). Springer Berlin Heidelberg. [https://doi.org/10.1007/978-3-642-85167-4\\_14](https://doi.org/10.1007/978-3-642-85167-4_14)
- Bonatesta, F., Chiappetta, E., & La Rocca, A. (2014). Part-load particulate matter from a GDI engine and the connection with combustion characteristics. *Applied Energy*, 124, 366–376. <https://doi.org/10.1016/j.apenergy.2014.03.030>
- Bunting, B. G., Wildman, C. B., Szybist, J. P., Lewis, S., & Storey, J. (2007). Fuel chemistry and cetane effects on diesel homogeneous charge compression ignition performance, combustion, and emissions. *International Journal of Engine Research*, 8(1), 15–27. <https://doi.org/10.1243/14680874JER01306>
- Charron, A., & Harrison, R. M. (2003). Primary particle formation from vehicle emissions during exhaust dilution in the roadside atmosphere. *Atmospheric Environment*, 37(29), 4109–4119. [https://doi.org/10.1016/S1352-2310\(03\)00510-7](https://doi.org/10.1016/S1352-2310(03)00510-7)
- Chen, L., Stone, R., & Richardson, D. (2012). A study of mixture preparation and PM emissions using a direct injection engine fuelled with stoichiometric gasoline/ethanol blends. *Fuel*, 96, 120–130. <https://doi.org/10.1016/j.fuel.2011.12.070>
- Clague, A. D., Donnet, J., Wang, T., & Peng, J. C. (1999). A comparison of diesel engine soot with carbon black. *Carbon*, 37(10), 1553–1565. [https://doi.org/10.1016/S0008-6223\(99\)00035-4](https://doi.org/10.1016/S0008-6223(99)00035-4)
- Davidson, C. I., Phalen, R. F., & Solomon, P. A. (2005). Airborne Particulate Matter and Human Health: A Review. *Aerosol Science and Technology*, 39(8), 737–749. <https://doi.org/10.1080/02786820500191348>
- Desantes, J. M., Bermúdez, V., García, J. M., & Fuentes, E. (2005). Effects of current engine strategies on the exhaust aerosol particle size distribution from a Heavy-Duty Diesel Engine. *Journal of Aerosol Science*, 36(10), 1251–1276. <https://doi.org/10.1016/j.jaerosci.2005.01.002>
- Desantes, J. M., Bermúdez, V., Pastor, J. V., & Fuentes, E. (2004). Methodology for measuring exhaust aerosol size distributions from heavy duty diesel engines by means of a scanning mobility particle sizer. *Measurement Science and Technology*, 15(10), 2083–2098. <https://doi.org/10.1088/0957-0233/15/10/019>
- Drews, P., Albin, T., Hoffmann, K., anegas, A., Felsch, Peters, N., & Abel, D. (2010). Model-Based Optimal Control for PCCI Combustion Engines. *IFAC Proceedings Volumes*, 43(7), 288–293. <https://doi.org/10.3182/20100712-3-DE-2013.00154>
- Fierz, M., & Burtscher, H. (2003). Separation of solid and volatile fraction by thermodesorption and hot dilution. In *7th ETH Conference on Combustion Generated Nanoparticles*. Zurich. Retrieved from [https://www.researchgate.net/publication/268399064\\_Separation\\_of\\_solid\\_and\\_volatile\\_fraction\\_by\\_thermodesorpti](https://www.researchgate.net/publication/268399064_Separation_of_solid_and_volatile_fraction_by_thermodesorpti)

on\_and\_hot\_dilution

- Frenklach, M., & Wang, H. (1994). Detailed Mechanism and Modeling of Soot Particle Formation (pp. 165–192). Springer Berlin Heidelberg. [https://doi.org/10.1007/978-3-642-85167-4\\_10](https://doi.org/10.1007/978-3-642-85167-4_10)
- Haynes, B. S., & Wagner, H. G. (1981). Soot formation. *Progress in Energy and Combustion Science*, 7(4), 229–273. [https://doi.org/10.1016/0360-1285\(81\)90001-0](https://doi.org/10.1016/0360-1285(81)90001-0)
- Hildingsson, L., Kalghatgi, G., Tait, N., Johansson, B., & Harrison, A. (2009). Fuel Octane Effects in the Partially Premixed Combustion Regime in Compression Ignition Engines. In *SAE Technical Paper. 2009-01-2648*. <https://doi.org/10.4271/2009-01-2648>
- Hinds, W. C. (1999). *Aerosol technology : properties, behavior, and measurement of airborne particles* (2nd ed). Wiley.
- Ickes, A. M., Bohac, S. V., & Assanis, D. N. (2009). Effect of fuel cetane number on a premixed diesel combustion mode. *International Journal of Engine Research*, 10(4), 251–263. <https://doi.org/10.1243/14680874JER03809>
- Jain, A., Singh, A. P., & Agarwal, A. K. (2017). Effect of fuel injection parameters on combustion stability and emissions of a mineral diesel fueled partially premixed charge compression ignition (PCCI) engine. *Applied Energy*, 190, 658–669. <https://doi.org/10.1016/j.apenergy.2016.12.164>
- Jia, M., Li, Y., Xie, M., & Wang, T. (2013). Numerical evaluation of the potential of late intake valve closing strategy for diesel PCCI (premixed charge compression ignition) engine in a wide speed and load range. *Energy*, 51, 203–215. <https://doi.org/10.1016/j.energy.2012.12.041>
- Kalghatgi, G. T., Risberg, P., & Angstrom, H.-E. (2007). Partially Pre-Mixed Auto-Ignition of Gasoline to Attain Low Smoke and Low NOx at High Load in a Compression Ignition Engine and Comparison with a Diesel Fuel. In *SAE Technical Paper. 2007-01-0006*. <https://doi.org/10.4271/2007-01-0006>
- Kasper, M. (2004). The Number Concentration of Non-Volatile Particles - Design Study for an Instrument According to the PMP Recommendations. In *SAE Technical Paper. 2004-01-0960*. <https://doi.org/10.4271/2004-01-0960>
- Kim, K.-H., Kabir, E., & Kabir, S. (2015). A review on the human health impact of airborne particulate matter. *Environment International*, 74, 136–143. <https://doi.org/10.1016/j.envint.2014.10.005>
- Kittelson, D. B. (1998). Engines and nanoparticles: a review. *Journal of Aerosol Science*, 29(5), 575–588. [https://doi.org/10.1016/S0021-8502\(97\)10037-4](https://doi.org/10.1016/S0021-8502(97)10037-4)
- Kittelson, D. B., Watts, W. F., & Johnson, J. P. (2006). On-road and laboratory evaluation of combustion aerosols Part1: Summary of diesel engine results. *Journal of Aerosol Science*, 37(8), 913–930. <https://doi.org/10.1016/j.jaerosci.2005.08.005>
- Kumar, P., Fennell, P., & Britter, R. (2008). Effect of wind direction and speed on the dispersion of nucleation and accumulation mode particles in an urban street canyon. *Science of The Total Environment*, 402(1), 82–94. <https://doi.org/10.1016/j.scitotenv.2008.04.032>
- Lapuerta, M., Armas, O., & Gómez, A. (2003). Diesel Particle Size Distribution Estimation from Digital Image Analysis. *Aerosol Science and Technology*, 37(4), 369–381. <https://doi.org/10.1080/02786820300970>
- Lapuerta, M., Armas, O., & Hernandez, J. J. (1999). Diagnosis of DI Diesel combustion from in-cylinder pressure signal by estimation of mean thermodynamic properties of the gas. *Applied Thermal Engineering*, 19(5), 513–529. [https://doi.org/10.1016/S1359-4311\(98\)00075-1](https://doi.org/10.1016/S1359-4311(98)00075-1)
- Maricq, M. M., Podsiadlik, D. H., Brehob, D. D., & Haghgoeie, M. (1999). Particulate Emissions from a Direct-Injection Spark-Ignition (DISI) Engine. In *SAE Technical Paper. 1999-01-1530*. <https://doi.org/10.4271/1999-01-1530>
- McCreanor, J., Cullinan, P., Nieuwenhuijsen, M. J., Stewart-Evans, J., Malliarou, E., Jarup, L., ... Zhang, J. (2007). Respiratory Effects of Exposure to Diesel Traffic in Persons with Asthma. *New England Journal of Medicine*, 357(23), 2348–2358. <https://doi.org/10.1056/NEJMoa071535>
- Mosbach, S., Celnik, M. S., Raj, A., Kraft, M., Zhang, H. R., Kubo, S., & Kim, K.-O. (2009). Towards a detailed soot model for internal combustion engines. *Combustion and Flame*, 156(6), 1156–1165. <https://doi.org/10.1016/j.combustflame.2009.01.003>
- Mueller, M. E., Blanquart, G., & Pitsch, H. (2009). Hybrid Method of Moments for modeling soot formation and growth. *Combustion and Flame*, 156(6), 1143–1155. <https://doi.org/10.1016/j.combustflame.2009.01.025>
- Noehre, C., Andersson, M., Johansson, B., & Hultqvist, A. (2006). Characterization of Partially Premixed Combustion. In *SAE Technical Paper. 2006-01-3412*. <https://doi.org/10.4271/2006-01-3412>
- Oberdörster, G., Oberdörster, E., & Oberdörster, J. (2005). Nanotoxicology: An Emerging Discipline Evolving from Studies of Ultrafine Particles. *Environmental Health Perspectives*, 113(7), 823–839. <https://doi.org/10.1289/ehp.7339>
- Okude, K., Mori, K., Shiino, S., & Moriya, T. (2004). Premixed Compression Ignition (PCI) Combustion for Simultaneous Reduction of NOx and Soot in Diesel Engine. In *SAE Technical Paper. 2004-01-1907*. <https://doi.org/10.4271/2004-01-1907>

- Park, S., Wang, Y., Chung, S. H., & Sarathy, S. M. (2017). Compositional effects on PAH and soot formation in counterflow diffusion flames of gasoline surrogate fuels. *Combustion and Flame*, 178, 46–60. <https://doi.org/10.1016/j.combustflame.2017.01.001>
- Payri, F., Molina, S., Martín, J., & Armas, O. (2006). Influence of measurement errors and estimated parameters on combustion diagnosis. *Applied Thermal Engineering*, 26(2–3), 226–236. <https://doi.org/10.1016/j.applthermaleng.2005.05.006>
- Pope, C. A., & Dockery, D. W. (2006). Health Effects of Fine Particulate Air Pollution: Lines that Connect. *Journal of the Air & Waste Management Association*, 56(6), 709–742. <https://doi.org/10.1080/10473289.2006.10464485>
- Rönkkö, T., Virtanen, A., Kannosto, J., Jorma Keskinen, Maija Lappi, A., & Liisa Pirjola. (2007). Nucleation Mode Particles with a Nonvolatile Core in the Exhaust of a Heavy Duty Diesel Vehicle. *Environ. Sci. Technol.*, 41(18), 6384–6389. <https://doi.org/10.1021/ES0705339>
- Saxena, M. R., & Maurya, R. K. (2017). Effect of premixing ratio, injection timing and compression ratio on nano particle emissions from dual fuel non-road compression ignition engine fueled with gasoline/methanol (port injection) and diesel (direct injection). *Fuel*, 203, 894–914. <https://doi.org/10.1016/j.fuel.2017.05.015>
- Seinfeld, J. H., & Pandis, S. N. (2006). *Atmospheric chemistry and physics: from air pollution to climate change* (2nd ed). Hoboken, New Jersey: John Wiley & Sons.
- Sellnau, M. C., Sinnamon, J., Hoyer, K., & Husted, H. (2012). Full-Time Gasoline Direct-Injection Compression Ignition (GDCI) for High Efficiency and Low NO<sub>x</sub> and PM. *SAE International Journal of Engines*, 5(2), 300–314. <https://doi.org/10.4271/2012-01-0384>
- Sgro, L. A., Sementa, P., Vaglieco, B. M., Rusciano, G., D'Anna, A., & Minutolo, P. (2012). Investigating the origin of nuclei particles in GDI engine exhausts. *Combustion and Flame*, 159(4), 1687–1692. <https://doi.org/10.1016/j.combustflame.2011.12.013>
- Singh, A. P., & Agarwal, A. K. (2012). Combustion characteristics of diesel HCCI engine: An experimental investigation using external mixture formation technique. *Applied Energy*, 99, 116–125. <https://doi.org/10.1016/j.apenergy.2012.03.060>
- Singh, G., Singh, A. P., & Agarwal, A. K. (2014). Experimental investigations of combustion, performance and emission characterization of biodiesel fuelled HCCI engine using external mixture formation technique. *Sustainable Energy Technologies and Assessments*, 6, 116–128. <https://doi.org/10.1016/j.seta.2014.01.002>
- Stanmore, B. ., Brillhac, J. ., & Gilot, P. (2001). The oxidation of soot: a review of experiments, mechanisms and models. *Carbon*, 39(15), 2247–2268. [https://doi.org/10.1016/S0008-6223\(01\)00109-9](https://doi.org/10.1016/S0008-6223(01)00109-9)
- Symonds, J. P. R., Price, P., Williams, P. I., & Stone, R. (2008). Density of particles emitted from a gasoline direct injection engine. In *12th ETH Conference on Combustion Generated Nanoparticles*. At Zurich. Retrieved from [https://www.researchgate.net/publication/261991364\\_Density\\_of\\_particles\\_emitted\\_from\\_a\\_gasoline\\_direct\\_injection\\_engine](https://www.researchgate.net/publication/261991364_Density_of_particles_emitted_from_a_gasoline_direct_injection_engine)
- Torregrosa, A. J., Broatch, A., García, A., & Mónico, L. F. (2013). Sensitivity of combustion noise and NO<sub>x</sub> and soot emissions to pilot injection in PCCI Diesel engines. *Applied Energy*, 104, 149–157. <https://doi.org/10.1016/j.apenergy.2012.11.040>
- Velji, A., Yeom, K., Wagner, U., Spicher, U., Rossbach, M., Suntz, R., & Bockhorn, H. (2010). Investigations of the Formation and Oxidation of Soot Inside a Direct Injection Spark Ignition Engine Using Advanced Laser-Techniques. In *SAE Technical Paper. 2010-01-0352*. <https://doi.org/10.4271/2010-01-0352>
- Wang, B., Mosbach, S., Schmutzhard, S., Shuai, S., Huang, Y., & Kraft, M. (2016). Modelling soot formation from wall films in a gasoline direct injection engine using a detailed population balance model. *Applied Energy*, 163, 154–166. <https://doi.org/10.1016/j.apenergy.2015.11.011>
- Weall, A., & Collings, N. (2009). Gasoline Fuelled Partially Premixed Compression Ignition in a Light Duty Multi Cylinder Engine: A Study of Low Load and Low Speed Operation. *SAE International Journal of Engines*, 2(1), 1574–1586. <https://doi.org/10.4271/2009-01-1791>
- Yao, M., Zheng, Z., & Liu, H. (2009). Progress and recent trends in homogeneous charge compression ignition (HCCI) engines. *Progress in Energy and Combustion Science*, 35(5), 398–437. <https://doi.org/10.1016/j.pecs.2009.05.001>
- Zhang, X., Wang, H., Zheng, Z., Reitz, R., & Yao, M. (2016). Experimental investigations of gasoline partially premixed combustion with an exhaust rebreathing valve strategy at low loads. *Applied Thermal Engineering*, 103, 832–841. <https://doi.org/10.1016/j.applthermaleng.2016.04.147>